AIP Conference Proceedings

STABILITY ANALYSIS OF THE ITER TF CONDUCTOR

Cite as: AIP Conference Proceedings **985**, 1269 (2008); https://doi.org/10.1063/1.2908482
Published Online: 27 March 2008

L. Savoldi Richard, and R. Zanino

STABILITY ANALYSIS OF THE ITER TF CONDUCTOR

L. Savoldi Richard, and R. Zanino

Dipartimento di Energetica, Politecnico
Torino, I-10129, Italy

ABSTRACT

The stability analysis of the reference Nb_3Sn conductor for the International Thermonuclear Experimental Reactor (ITER) Toroidal Field (TF) coils is performed using the Mithrandir code. From the point of view of the temperature margin, the most critical conductor in the winding pack, as well as the most critical location along it, is identified by a Vincenta code analysis, which also provides the initial and boundary conditions for the stability study. With this approach, the 1D Mithrandir analysis can be restricted to the most critical conductor, using a much finer grid than Vincenta, in order to capture the details of normal zone initiation and possible recovery to SC state. Two different disturbances are considered: one short in space and time (0.01 m, 1 ms), simulating a disturbance of mechanical nature, the other longer (3 m, 100 ms), corresponding to AC losses (plasma disruption). Both disturbances are applied to the superconducting cable at end-of-burn, in the reference ITER inductive operation scenario. The grid-independence of the results was verified first. Since the results are strongly influenced by the choice of the heat transfer coefficient between strands and helium, this effect has been also parametrically investigated. In all cases, the computed minimum quench energies turn out to be above the level of the expected disturbances.

KEYWORDS: Fusion reactors, ITER, Superconducting magnets, Stability, Computational methods.

INTRODUCTION

The present work concerns the 1D thermal-hydraulic simulation of the ITER TF coils at the conductor level using the Mithrandir code [1], with the main aim of updating the ITER conductor design documentation. In the present ITER design, each TF coil will be

CP985, *Advances in Cryogenic Engineering: Transactions of the Cryogenic Engineering Conference—CEC, Vol. 53,* edited by J. G. Weisend II

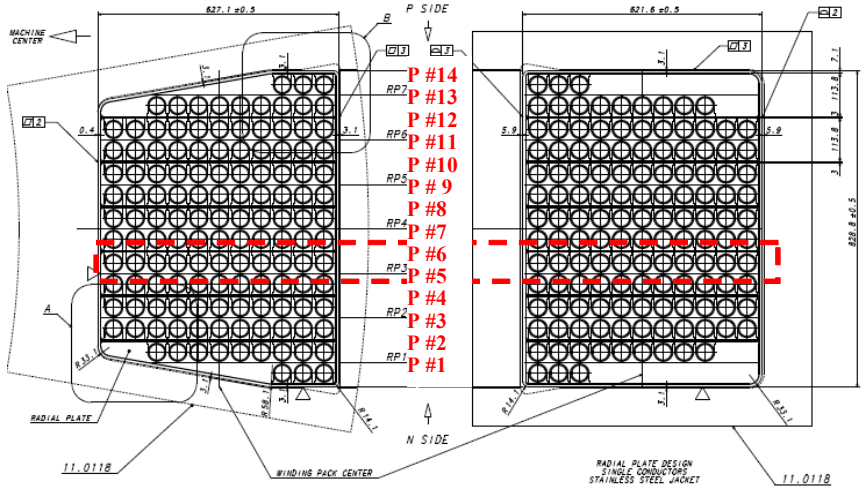

FIGURE 1. TF coil cross section (ITER Documentation, Drawing Number 11.0102.0018) showing the inboard and outboard legs (left and right, respectively).

wound in double-pancakes on a radial plate as seen in FIGURE 1. Each conductor is a two-channel Cable-In-Conduit Conductor (CICC) with a thin SS jacket. The TF pancakes, cooled by supercritical helium (SHe) at ~4.5 K and 0.5 MPa, are numbered 1 through 14. Adjacent pancakes are poloidally cooled, alternating clock-wise/counter-clockwise direction due to the double-pancake winding configuration, with the helium inlet located at the conductor joggle of the innermost turn.

Based on the Vincenta analysis [2], performed only on the first 7 pancakes assuming symmetry, pancake #6 was selected for the present stability study as it shows the highest electric field, and therefore the lowest temperature margin, at the end of burn (EOB) of the plasma reference inductive operation, with a flat top current of 15 MA.

Two stability disturbances are considered here, one corresponding to a mechanical disturbance and the other to a plasma disruption. Conservatively, the disturbance is applied at the conductor location where the margin is the lowest, i.e. at the bottom of the inboard leg, at EOB (time t = 530 s).

The results presented below might in principle be compared with both the original

TABLE 1. Main data of the ITER TF conductor used as input in the present simulations [5]

Strand parameters	**Value**
Superconducting (SC) material	Nb_3Sn
# of strands (SC, Cu)	900, 522
Cu : non-Cu (SC strands)	1.0
RRR	100
Conductor parameters	**Value**
# of strands (SC, Cu)	900, 522
Cabling pattern	((2sc+1Cu) × 3 × 5 × 5+core) × 6
Cosθ	0.95
Conductor length	379.08 m
Void fraction	33.2 %
∅ central channel (ID × OD)	7 mm × 9 mm
Central channel nominal perforation	25 %
∅ jacket (ID × OD)	40.5 mm × 43.7 mm
Jacket material	316LN
Petal wrapping wetted perimeter	330 mm

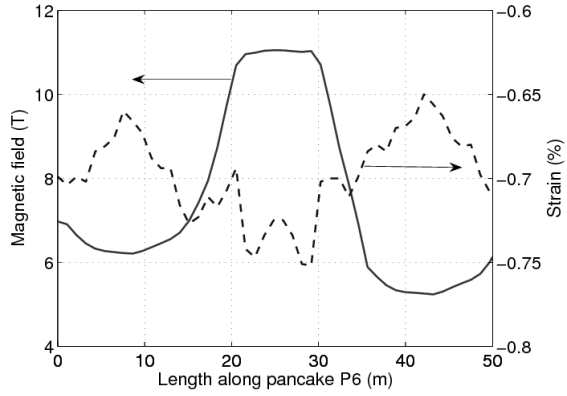

FIGURE 2. Spatial profile of the magnetic field (solid line, left axis) and longitudinal strain in the filaments (dashed line, right axis) along the first 40 m of TF pancake #6 at EOB, used as input in the simulations.

documentation [3] and with more recent work [4], but this comparison will not be attempted here in view of the (too) many differences in the tools and input used. A careful numerical convergence study has been performed, however, to confirm the accuracy of the present analysis.

SIMULATION SET-UP

As prescribed in [5], only the Cu in the superconducting strands is accounted for in the simulations, and the helium in the central channel is considered unavailable for the strand cooling by setting the heat transfer coefficient between annulus and hole to zero in the Mithrandir input [1]. In the model, however, the helium in the bundle can still be exhausted to the central channel via the perforation.

The following input has been used for the simulations:

- Strand and conductor. The non-copper critical current density J_C is computed as a function of the magnetic field B, the temperature T and the total longitudinal intrinsic strain of the Nb_3Sn filaments in the strand ε, using the Summers scaling law [6] with a correction to avoid the discontinuity at zero field B, as prescribed in [5]. The scaling parameters are selected as: T_{c0m} = 18 K, B_{c20m} = 28 T, $C_{00} = 1.303\times10^{10}$ A/mm^2, giving j_C = 800 A/mm^2 as a reference value at 12 T, 4.2 K, ε = –0.25%. The cable n-value n = 7 is used in the simulations [5]. The reference conductor data used for our simulations are reported in TABLE 1.
- Magnetic field and strain. The operating current in the TF coils is 68 kA. The magnetic field distribution and the longitudinal strain in the superconducting filaments, computed along the conductor axis, are shown in FIGURE 2 at the EOB. The magnetic field reaches its peak values (~11 T) between ~20 m and ~30 m from the conductor inlet, i.e., along the straight leg of the inner turn. The strain data were obtained adding the three components $\varepsilon_{th} + \varepsilon_{op} + \varepsilon_{extra}$ [4] consistently with the selected J_C scaling. The most compressive strain is found near the end of the straight vertical leg, corresponding to the magnetic field plateau at ~11 T. In these conditions the current sharing temperature T_{CS} is ~5.5 K, if computed with the maximum field, or ~6.1 K, if computed with the average field.
- Heat load and transfer coefficients. The "background" heat load along the conductor axis (including AC losses in the conductor + eddy current + losses in the structure,

TABLE 2. Location, length and duration of the disturbance scenarios applied to the ITER TF conductor.

	Mechanical disturbance	**Plasma disruption**
Location	Peak electric field (x = 29 m)	Highest average electric field (26.5 m < x < 29.5 m)
Length L_D	0.01 m	3 m
Duration τ_D	1 ms	100 ms

thermal radiation, thermal conduction and nuclear heating) was computed using the Vincenta code. The peak value (~1.5 W/m) is reached along the straight leg of the inner turn.

Different heat transfer coefficients $h_{St\text{-}He}$ between strands and helium are used in the simulations (the Kapitza thermal resistance is accounted for in all cases, but it has a negligible impact in the temperature range of TF coil operation):

- We first consider conservatively the steady-state value (i.e., no transient heat transfer coefficient accounted for in the reference case). This is based on the Dittus-Boelter correlation, with a lower bound for the Nusselt number (corresponding to the laminar limit, assumed here as $Nu_{lim} = 8.23$), giving $h_{St\text{-}He}$ ~450 W/m^{2}K. In the operating conditions of the ITER TF, this limit is typically *not* overcome, at least not until a significant acceleration of the helium flow occurs (e.g., because of heat deposition). The sensitivity to the value of the Nu lower bound Nu_{lim}, which depends on the flow geometry and is rather uncertain in our case, should also be investigated in the future.
- The effect of a parametric variation from (constant) $h_{St\text{-}He}$ = 500 W/m^{2}K to 5000 W/m^{2}K was evaluated next (the latter was the value retained for the previous analysis of stability in the CS Insert Coil [7]).
- The effect of a transient heat transfer coefficient, not included in the nominal analysis, was finally analyzed.

- Initial and boundary conditions. The boundary conditions on temperature and pressure during the entire plasma scenario are provided by the Vincenta analysis, which accounts in particular for the presence of the different hydraulic paths (pancakes) in parallel. The initial condition for the stability analysis has been computed self-consistently by Mithrandir following the plasma scenario for the first 530 s. The temperature profile along the strands at EOB is shown in FIGURE 3a, showing a peak at ~29 m. The boundary conditions are kept fixed at T_{in} = 4.4 K, p_{in} = 0.595 MPa, p_{out} = 0.499 MPa, which is justified by the relatively short timescales of the stability disturbance applied here.

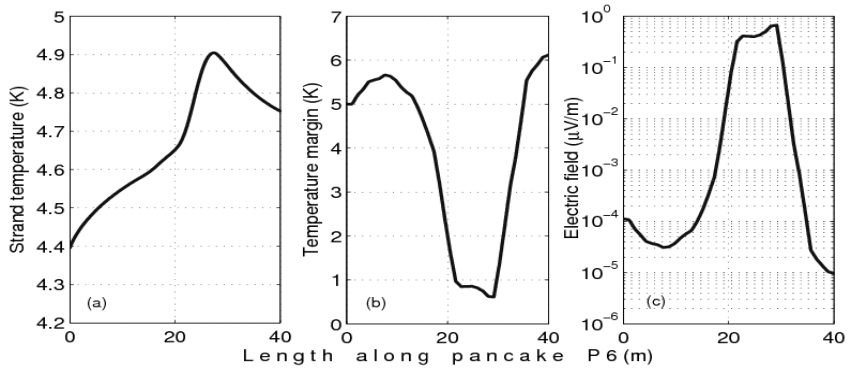

FIGURE 3. Spatial profile of (a) the strand temperature, (b) the temperature margin (= $T_{CS} - T_{strand}$ @ B_{peak}) and (c) electric field computed by Mithrandir along the first turn of TF pancake #6 at EOB.

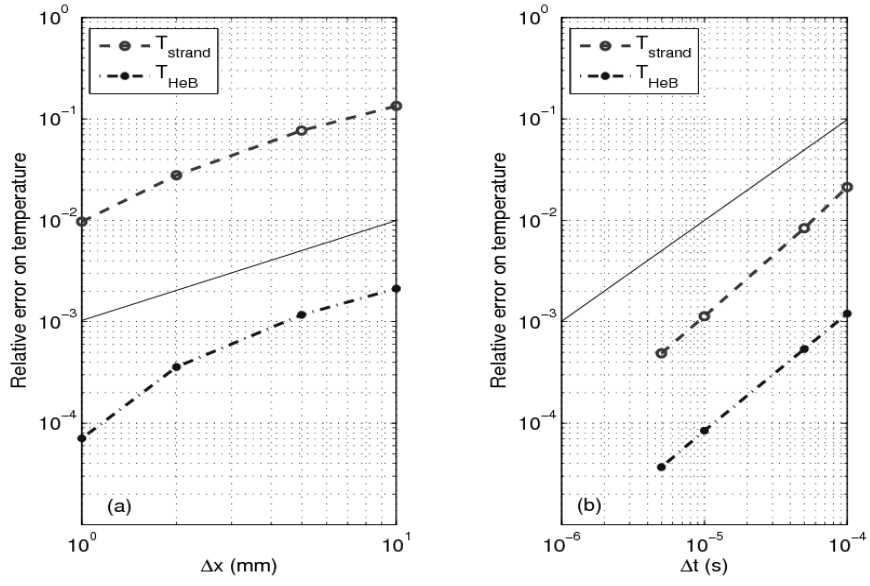

FIGURE 4. Mechanical disturbance: (a) space convergence analysis on strand (dashed) and bundle helium (dash-dotted) temperature @ x = 29.01 m (end of the heated zone), t = 0.001 s after the EOB (end of the heating), Δt = 5 μs. (b) Time convergence analysis on strand (dashed) and bundle helium (dash-dotted) temperature @ x = 29.01 m (end of the heated zone), t = 0.001 s after the EOB (end of the heating), Δx = 1 mm. The solid lines represent the ideal slope of the error.

- Disturbance scenarios. Two disturbances of different origin (mechanical and plasma disruption) are used as drivers for the stability transients, see TABLE 2, dissipating heat (assumed to be uniform on the cross section [8]) directly in the SC strands. As mentioned above, all three parameters B, T, ε reach their most critical condition along the vertical straight leg, which then shows the lowest temperature margin. The temperature margin computed along the first turn at EOB is reported in FIGURE 3b. The minimum margin, which corresponds to the maximum electric field (see FIGURE 3c), appears at x ~29 m, where the mechanical disturbance, for instance, will be thus applied to the conductor.
- Numerics. The stability simulations have been performed using:
  - The fully implicit time scheme for the mechanical disturbance, the Crank-Nicolson time scheme for the plasma disruption disturbance (the Jacobian being, roughly speaking, inversely proportional to $(\Delta x)^2$, see below);
  - An upwind spatial scheme for the advective terms;
  - A refined mesh around the disturbance region, with constant element size Δx in the refined region (the outer region is never reached by the normal zone on the stability timescale, so that it has no influence here);
  - A constant time step Δt.

  A detailed space and time convergence study has been carried out, as suggested in [5], and the results are reported in FIGURE 4 for the most critical, mechanical disturbance. In the worst case, the estimated relative error of the hydraulic and thermal variables is ~1 %, for both the simulation of mechanical disturbance with Δx = 0.001 m and Δt = 5 μs, and the simulation of a plasma disruption with Δx = 0.01 m and Δt = 100 μs. These values of Δx and Δt have been therefore retained for the

analysis below. For both disturbances, also the ideal slopes of the different methods in space and time are recovered by the numerical solution, confirming convergence, see e.g. FIGURE 4.

RESULTS

The search of the minimum quench energy (MQE) and of the maximum recovery energy (MRE) has been performed automatically. The simulations end with a quench when the computed voltage along the conductor exceeds 0.1 V, whereas they end with a recovery when the local electric field is everywhere < 10 μV/m after the end of the disturbance. The overall results of the simulations are summarized in TABLE 3, details are discussed below.

The following analysis is 1D in nature, as mentioned above. However, the transit time of the SHe is longer than the relevant time scales for recovery/quench decision for both disturbances, so that only the helium initially under the normal zone can be considered available in principle.

Mechanical Disturbance

The results are reported in FIGURE 5 a, c, e in terms of evolution of the total voltage across the conductor and of the strand temperature and bundle helium temperature at the end (downstream) of the heated region, for both MRE and MQE (63-66 mJ/ccst, respectively). One can see that the voltage does not decrease right after the end of the disturbance, notwithstanding the immediate drop of the strand temperature. This is due to an increase in the normal zone length (not shown).

It may also be noted that the strand temperature increases much faster than the helium temperature (i.e., it is somehow decoupled from it). Indeed, during the external heating phase of the transient the cooling capacity of the helium is very poor compared to the external heating source, whereas it is comparable to the Joule heating; the latter remains as only source after the end of the disturbance, so that the recovery/quench decision can be made on a timescale longer than the disturbance duration.

In the recently discussed [9] modified design of the ITER TF conductor, a significant reduction of the void fraction in the annulus combined with an increased central channel diameter lead to an almost reversed repartition of the mass flow rate in the two regions, compared to the reference design used in the present calculation. However, this has hardly an influence on the computed margin, since for this disturbance the role of the helium is very limited (ill-cooled regime, see below).

Plasma Disruption Disturbance

The results are reported in FIGURE 5 b, d, f, for both MRE and MQE (440-460

TABLE 3. Computed energy margin for different $h_{St\text{-}He}$

$h_{St\text{-}He}$ (W/m^{2}K)	Mechanical disturbance MRE-MQE (mJ/ccst)	Plasma disruption MRE/MQE (mJ/ccst)
Steady-state (Dittus-Boelter)	63-66	440-460
500	66-70	440-460
1000	860-900	650-700
Transient + Steady-state (Dittus-Boelter)	640-700	440-460

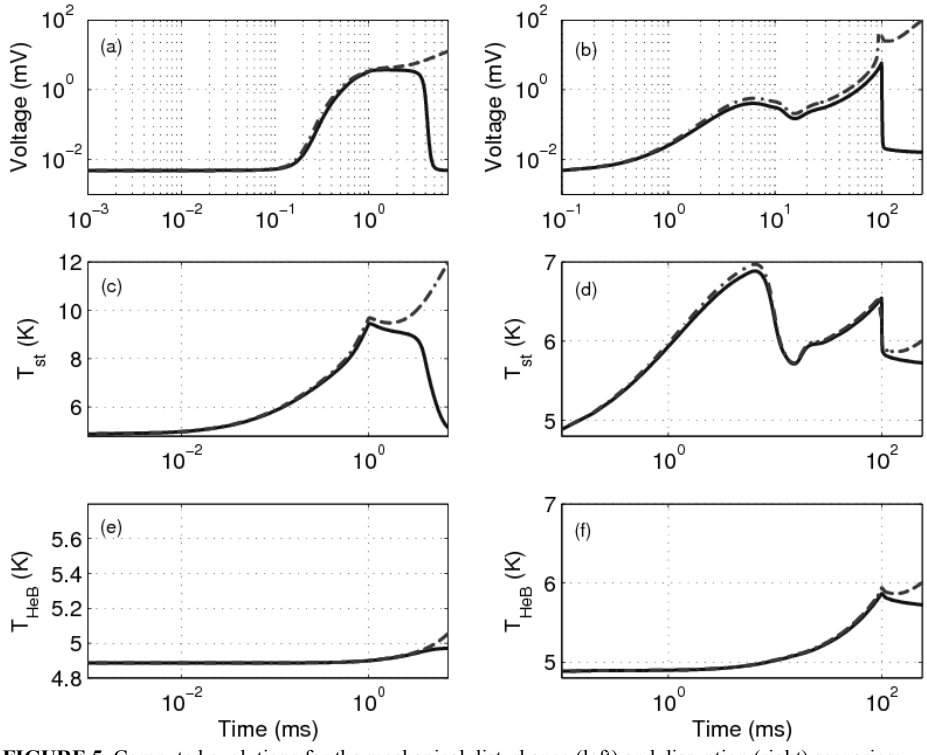

FIGURE 5. Computed evolutions for the mechanical disturbance (left) and disruption (right) scenarios: voltage along P6 (a),(b), strand temperature (c),(d) and bundle helium temperature (e),(f) at the end of the heated zone, for the MQE (dashed lines) and MRE (solid lines) respectively.

mJ/ccst, respectively).

The computed voltage across the conductor evolves non-monotonically during the heating, following the behavior of the strand temperature. This is in turn driven by the increase in heat transfer coefficient driven by the heating-induced flow (Reynolds number dependence in Dittus-Boelter correlation).

Since in this case the disturbance duration allows the bundle helium to be thermally coupled to the strands, the decision on recovery/quench can be taken on a timescale comparable to the duration of the disturbance heating.

Parametric Effect of $h_{St\text{-}He}$

The increase of $h_{St\text{-}He}$ from 500 W/m^{2}K to 1000 W/m^{2}K gives a dramatic effect on the computed margin for a mechanical disturbance, which increases by a factor of ~10-15, as reported in TABLE 3. This is due to the fact that the limiting current [10] for $h_{St\text{-}He}$ = 500 W/m^{2}K and 1000 W/m^{2}K can be computed as ~59 kA and ~83 kA, respectively. Being the transport current 68 kA, in the former case the strands are in the ill-cooled regime, while in the latter they are in the well cooled regime [11]. On the contrary, the increase of $h_{St\text{-}He}$ gives only a weak increase in the energy margin, if the disruption disturbance is considered, in view of its long duration.

The inclusion of a transient contribution h_t in $h_{St\text{-}He}$ (the recipe for constant wall temperature was chosen here) practically acts (for a limited time, though, ~10-15 ms) as would an increased value of $h_{St\text{-}He}$, so that its effects are similar to those just discussed for

the mechanical disturbance, while no effect is detected on the longer plasma disruption time scale, see TABLE 3.

CONCLUSIONS

In the most conservative simulation, i.e., considering only the steady-state heat transfer coefficient between strand and helium with a laminar limit for the Nusselt number set at ~8, the computed stability margin for the mechanical disturbance is ~5-10 times higher than the expected disturbance reported in [8]. This (safety) factor increases by 1 order of magnitude, if transient heat transfer is considered. As a consequence, the TF conductor should not suffer from quenches initiated by mechanical disturbances.

As far as a plasma disruption in concerned, the estimate of the peak local conductor losses generated during a plasma disruption can be found in [12]. Again, in the most conservative simulation, the computed stability threshold is ~1-2 orders of magnitude higher than the estimated loss, giving confidence that the TF conductor should not suffer from quenches initiated by a plasma disruption either.

While these results indicate that, for instance, a lower Cu : nonCu could be sufficient from the stability point of view, the value of 1.0, see TABLE 1, is still maintained as an empirical limit in the ITER conductor design [5].

ACKNOWLEDGEMENTS

This work was partially supported by the European Fusion Development Agreement under contract EFDA/05-1364. We thank D. Bessette for providing the input data and the results of the Vincenta calculations referred to in the text.

REFERENCES

1. Zanino, R., De Palo, S., and Bottura, L., *J. Fus. Energy* **14**, pp. 25-40, (1995).
2. Bessette, D., Shatil, N., and Zapretilina, E., *IEEE Trans. Appl. Supercond.* **16**, pp. 795-799, (2006).
3. H. Takigami, "Gandalf analysis. The thermohydraulic simulation results", in ITER Design Description Document. Magnet: Section 2.1: Conductor design and analysis, Annex 10, N 11 DDD 140 01-07-12 R 0.1 (2001).
4. Y. Takahashi, K. Yoshida, Y. Nabara, M. Edaya, D. Bessette, N. Shatil and N. Mitchell, *IEEE Trans. Appl. Supercond.* **17**, (2007), to appear.
5. ITER Design Description Document. Magnet: Section 1: Engineering description, N 11 DDD 178 04-06-04 R 0.4 (2004).
6. Summers, L.T., Guinan, M.W., Miller, J.R., and Hahn, P.A., *IEEE Trans. Magn.* **27**, pp. 2041-2044, (1991).
7. Zanino, R., Carpaneto, E., Portone, A., Salpietro, E., and Savoldi, L., "Inductively driven transients in the CS Insert Coil (I): Heater calibration and conductor stability tests and analysis", in *Advances in Cryogenic Engineering* 47, edited by J. G. Weisend II et al., Plenum, New York, 2002, pp. 415-422.
8. Magnet Superconducting and Electrical Design Criteria, Annex to Design Requirements and Guidelines Level 1 (DRG1), N 11 MA 2 04-04-27 R 0.1 (2004).
9. Bessette, D., "Change of the Reference TF Conductor (Performance Qualification Samples)", ITER Conductor Meeting, EPFL/CRPP, Villigen, Switzerland, July 2-3, 2007.
10. Dresner, L., *IEEE Trans. Magn.*, MAG-17 pp.753-756, (1981).
11. J. Schultz and J. Minervini, "Sensitivity of energy margin and cost figures of internally cooled cabled superconductors (ICCS) to parametric variations in conductor design", M.I.T. Plasma Fusion Center Report PFC/JA-85-30.
12. ITER Design Description Document. Magnet: Section 2.1 Conductor Design and Analysis, N 11 DDD 156 01-07-13 R 0.1 (2001).